Effect of Chain Stiffness on Polymer Phase Behavior

Y.-J. Sheng and A. Z. Panagiotopoulos*

School of Chemical Engineering, Cornell University, Ithaca, New York 14850-5201

S. K. Kumar

Department of Materials Science and Engineering, The Pennsylvania State University, University Park, Pennsylvania 16802

Received September 8, 1995
Revised Manuscript Received March 4, 1996[⊗]

Introduction

Freely-jointed chain models have often been used to study thermodynamic properties of polymers including phase diagrams[1−5] and mechanical properties.[6−10] These models are efficient for describing the universal, long-range properties of chains. However, they are found[7] to be incapable of capturing some important structural details on monomeric length scales, since they have unrealistic flexibility on short-length scales. Fully flexible chains can bend back on themselves easily; thus, an individual site is likely to find itself embedded in a sea of intramolecular neighbors which effectively exclude sites on other chains from the neighboring vicinity. Unlike freely-jointed chain models which have no inherent stiffness, real polymeric chains have local stiffness caused by bond bending and rotational and torsional angles constraints. As the local stiffness is increased, intramolecular screening is reduced and interior sites become much more open to intermolecular contacts.

It is now well-known that phase behavior of polymeric systems is sensitive to subtle variations in molecular architecture.[11−14] For example, Yethiraj *et al.*[12] found that for an athermal binary polymer blend with stiffness disparity near a surface, at meltlike densities, the stiffer component always segregates preferentially to the surface. Bates *et al.*[13] and Liu and Fredrickson[14] have also shown that a difference in chain flexibility in a binary polymer blend can result in a substantial shift in the critical points and phase boundaries. Honnell *et al.*[7] have explored the effects of chain stiffness on the intermolecular structure of homopolymer melts. The influence of chain stiffness on the phase behavior of polymer chains, however, is still unclear. Since intermolecular contacts increase in number as chain stiffness increases, one may expect an increase in critical temperatures for the semiflexible chains over the freely-jointed chains. To resolve these issues, we have determined vapor−liquid equilibrium diagrams of a semiflexible chain model by a Monte Carlo method.[2] Vapor−liquid equilibria are experimentally relevant for chains of up to several tens of backbone carbon atoms.[15] The qualitative features of the vapor−liquid phase diagrams in one component chain systems are also similar to liquid−liquid phase diagrams for binary systems of polymer and solvent that exhibit an upper critical solution temperature. Chain chemical potentials were calculated more efficiently than in our previous study,[2] using a combination of the chain increment[16] and configurational-bias methods.[17,18,20] The phase behavior for a fully flexible bead−spring polymeric chain has already been obtained in our previous work.[2] By comparing the phase behavior of these two chain models, we clarify how the phase envelopes change due to chain stiffness.

Monte Carlo Simulations

Model. The fully flexible chains in our previous work were modeled as sequences of spherical segments connected by stiff springs.[2] The semiflexible chains studied here have the same spring potential for bonded beads. Nonbonded interactions for segments in different chains and segments separated by more than three bonds are also the same as the fully flexible chains, namely, Lennard-Jones (6,12) potentials with energy parameter ϵ and size parameter σ. The monomeric Lennard-Jones size and energy parameters are used to reduce all quantities reported (e.g., $T^* = k_B T/\epsilon$, $P^* = P\sigma^3/\epsilon$, where k_B is Boltzmann's constant). Beads on the same chain that are two and three bonds away interact via Lennard-Jones potentials in the flexible chain model used in our previous study, while their interaction is incorporated in the torsional potential for the semiflexible chains. This difference in intramolecular interactions is not likely to affect our conclusion since it only implies an effectively stiffer spring for the semiflexible chains. Chain stiffness is introduced explicitly through bond bending and torsional angle potentials. The valence angle, θ, between successive pairs of bonds is maintained close to the tetrahedral value θ_0 =109.47° by a potential quadratic in cos θ_0,

$$U_\theta = {}^1/_2 k_\theta(\cos\theta - \cos\theta_0)^2 \tag{1}$$

where $k_\theta/\epsilon = 20$. ϵ is the potential well depth for each segment of the chain, which interacts with distant segments via the standard (12,6) Lennard-Jones potential. Segmental Lennard-Jones parameters are used to reduce all quantities reported here to nondimensional form. The torsional angle, defined by three successive bonds, is constrained to lie mainly in *trans* and *gauche* rotational states by a 3-fold torsional potential,[19]

$$U_\phi = k_\phi \sum_{n=0}^{5} a_n \cos^n \phi \tag{2}$$

where $k_\phi/\epsilon = 1.8$, $a_0 = 1$, $a_1 = 1.310$, $a_2 = -1.414$, $a_3 = -0.3297$, $a_4 = 2.828$, and $a_5 = -3.3943$.. Constants a_0−a_5 are taken from ref 19. The parameters of the semiflexible chain model used here do not correspond to any specific known polymer system, since we have kept the bonded and nonbonded interaction potentials the same as the fully flexible model bead−spring chains.

Methods. Vapor−liquid phase equilibrium diagrams of the semiflexible chains are determined by methods similar to those of ref 2. However, calculations of the chemical potentials for the polymer chains were performed in this work through a combination of the chain increment method[16] with configurational-bias sampling.[17,18,20] Figure 1 presents the variation of incremental chemical potential $\mu_r^+(n)$ versus chain length n for growing a single chain of variable length in a medium of 20-mers at a liquid-like density obtained from constant-pressure simulations at reduced pressure $P^* = 0$ and reduced temperature $P^* = 2.5$. The volume fraction corresponding to these conditions is $\varphi = 0.53$, where $\phi = n\rho^*$, n is the chain length and $\rho^* = \rho\sigma^3$ is the reduced number density. The incremental chemical potential is the difference in chemical potentials between chains of length x and $x - 1$ and can be calculated to a high accuracy, even for a dense liquid. The chain length dependence of the chemical potential for the semiflexible chains is stronger than for the flexible chains in the short-chain region. Still, the incremental chemical potentials level off after the first few beads. This is in contrast to what was observed by de Pablo *et al.*[20] The simulations they performed were for isolated swollen chains, and they found

* To whom correspondence should be addressed. E-mail: azp2@cornell.edu.
⊗ Abstract published in *Advance ACS Abstracts,* May 1, 1996.

S0024-9297(95)01343-X CCC: $12.00

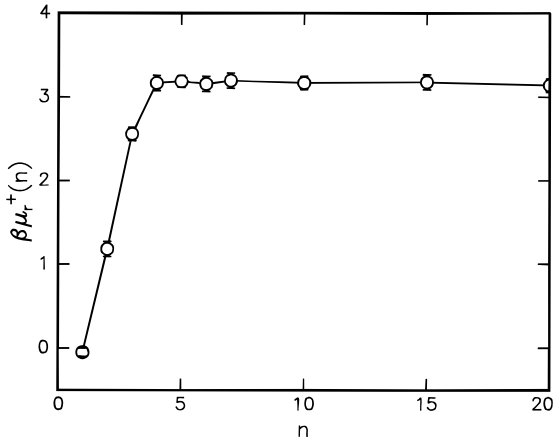

Figure 1. Incremental chemical potential, $\beta\mu_r^+(n)$, for a single growing semiflexible chain in a medium of 20-mers at reduced temperature $T^* = 2.5$ and reduced pressure $P^* = 0$, as a function of chain length n. Points are the Monte Carlo simulation results. Lines are drawn through the points for visual clarity. Incremental chemical potentials presented in this figure are calculated by the chain increment method.[16]

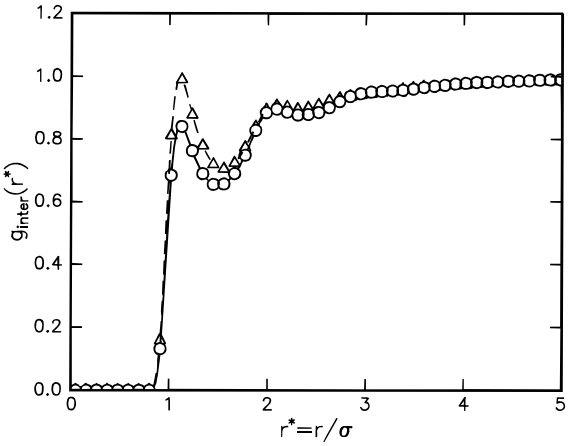

Figure 2. Intermolecular radial distribution function, $g_{inter}(r^*)$, for flexible and semiflexible 20-mers at volume fraction $\varphi = 0.65$ and reduced temperature $T^* = 2.5$. Monte Carlo results: (○) flexible chains; (△) semiflexible chains. Spline lines are drawn through the points for visual clarity.

Table 1. Phase Coexistence Envelope for Semiflexible Chains of Length n = 20, 50, and 100[a]

$n = 20$			$n = 50$			$n = 100$		
T^*	φ_{liq}	φ_{gas}	T^*	φ_{liq}	φ_{gas}	T^*	φ_{liq}	φ_{gas}
2.3	0.55(1)	3×10^{-4}	2.7	0.51(1)	3×10^{-4}	2.8	0.50(1)	7×10^{-6}
2.5	0.53(1)	6×10^{-3}	2.9	0.44(1)	2×10^{-3}	3.0	0.44(2)	9×10^{-5}
2.7	0.46(2)	1×10^{-2}	3.1	0.36(2)	7×10^{-3}	3.2	0.37(2)	5×10^{-4}
2.8	0.42(2)	2×10^{-2}	3.2	0.32(2)	1×10^{-2}	3.3	0.34(2)	1×10^{-3}
2.9	0.36(3)	4×10^{-2}	3.3	0.30(3)	2×10^{-2}	3.4	0.30(3)	3×10^{-2}
3.0	0.27(3)	5×10^{-2}				3.6	0.27(2)	8×10^{-3}

[a] The table lists the reduced temperature, $T^* = k_B T/\epsilon$, and volume fraction, $\varphi = n\rho\sigma^3$, where ρ is the molar density.

that the chain length dependence of the incremental chemical potentials on densities and temperatures was strong. For polymeric systems at high density, the incremental chemical potentials are less dependent of chain length. In order to include correctly the chain length dependence of the chain chemical potential, in our previous work[2] we have performed simulations to estimate the incremental chemical potentials of the first few beads, $\mu_r^+(i)$ ($i = 1-10$), and the asymptotic value, $\mu_r^{+,asym}$. Thus, for a chain of length n, the chain chemical potential can be approximately by

$$\mu_r^{chain}(n) = \sum_{i=1}^{l} \mu_r^+(i) + (n - l)\mu_r^{+,asym} \qquad (3)$$

In this work, we calculate the chemical potential of a short chain (beads $1 - l$), $\mu_r^{chain}(l)$, by using the configuration-bias method to insert a chain of length l. In the same simulation run, we use the chain increment method to find the asymptotic incremental chemical potential value. So, the chain chemical potential can be approximated as

$$\mu_r^{chain}(n) = \mu_r^{chain}(l) + (n - l)\mu_r^{+,asym} \qquad (4)$$

For all of the temperatures we have studied, the variation of incremental chemical potential with chain length shows behavior similar to that in Figure 1. The incremental chemical potentials level off around the fourth bead. We used $l \approx 7$ for this work to ensure that short-chain effects are properly taken into account. The chain chemical potential of an n-mer calculated in this way can be done in a single simulation. The combination of the chain increment and configurational-bias methods saves computational time and avoids accumulation of errors. We have performed constant-pressure simulations, for which the value of the pressure is an input parameter to the simulation and the equilibrium density is obtained as an average over the production period of a run. To obtain the phase diagrams, we used the iterative procedure of matching chemical potentials and pressures of the liquid and gas phases described in ref 2.

Results and Discussion

Figure 2 shows the intermolecular radial distribution functions, $g_{inter}(r^*)$, for the fully flexible and semiflexible homopolymeric melt at the same temperature ($T^* = 2.5$) and volume fraction ($\varphi = 0.65$). This volume fraction corresponds to a fairly dense liquid, as the volume fraction of the monomeric Lennard-Jones fluid at its triple point is[21] $\varphi = \rho^* = 0.87$. The bond bending and torsional angle potentials force the semiflexible chain to open up and have more interchain interactions than the bead−spring chains. At this liquid-like density, local structure exhibits a similar pattern to that of a simple monatomic fluid. The function $g_{inter}(r^*)$ increases rapidly from a value of zero to its peak value in the vicinity of $r/\sigma = 1$ and then oscillates on the short-length region. However, unlike simple fluids, over longer distances ($2 < r/\sigma < 4-5$), the curves approach a value of 1 rather slowly, leaving a long-range correlation "hole" indicating that intramolecular screening results in relative absence of intermolecular neighbors. These results are consistent with the findings of Honnell *et al.*[7]

The first-shell peak of $g_{inter}(r^*)$ is higher for the semiflexible system. This suggests that there are more intermolecular contacts for the semiflexible system, which in term may seem to suggest that the semiflexible system should have a higher critical temperature. In fact, better understanding of these systems can be achieved through the calculation of pressure due to intermolecular interactions since intermolecular contacts give both repulsive and attractive contribution to the pressure. We found that, at the same temperature and density, semiflexible chain systems always exhibit larger pressure than the flexible chain systems. We also find that, at the same density, the semiflexible chains have a higher volatility (vapor pressure) and higher chain chemical potentials than the flexible chains. Similar trends were obtained in ref 22.

As a result of the different volatility and pressures, rather different phase diagrams are observed for these two chain models. Table 1 gives the properties of the coexistence phases of the semiflexible chains. Figure 3

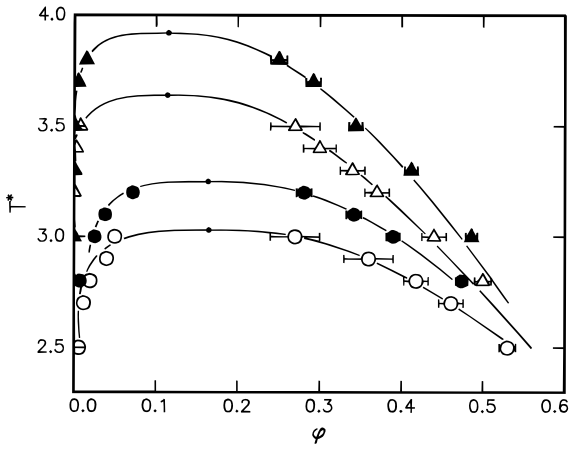

Figure 3. Reduced temperature, T^*, versus volume fraction, φ, at coexistence. Monte Carlo results: semiflexible chains, (○) $n = 20$, (△) $n = 100$; flexible chains, (●) $n = 20$, (▲) $n = 100$. Fitting of Monte Carlo results to scaling relationships with $\beta = 0.332$ (—).

Table 2. Estimated Critical Temperatures and Critical Volume Fractions for Semiflexible and Flexible Chains of Length $n = 20$, 50, and 100 using the Scaling Relationships[2] with $\beta = 0.332$

	semiflexible		flexible	
n	T_c^*	φ_c	T_c^*	φ_c
1	1.32	0.304	1.32	0.304
20	3.03	0.165	3.25	0.164
50	3.40	0.140	3.65	0.134
100	3.64	0.114	3.92	0.115
∞	4.25	0.0	4.59	0.0

shows the calculated vapor−liquid phase diagrams of the bead−spring chain model[2] and the semiflexible chain model for chain lengths $n = 20$ and 100. Results for $n = 50$ are not shown to avoid cluttering the figure, but the behavior is intermediate between $n = 20$ and 100. The coexistence curves of the semiflexible chains fall below and within the coexistence curves of the flexible counterparts. Critical points (shown in Table 2) are estimated by fitting the results for liquid and vapor densities to the rectilinear diameter rule and the scaling relationship, $\rho_{liq} - \rho_{gas} \propto (T_c - T)^{\beta}$ for the width of the coexistence curve. Consistent with previous practice,[2] we chose $\beta = 0.332$. The critical temperature for infinite chain length, T_c^{∞}, for the semiflexible model is estimated by extrapolation to zero abscissa in the Schultz−Flory diagram ($1/T_c^*$ versus $1/n^{1/2} + 1/2n$). The diagram results in a straight line and gives $T_c^{\infty} = 3.98$, about 7% lower than the corresponding flexible model.

Conclusion

We have calculated vapor−liquid phase diagrams of a semiflexible chain model using Monte Carlo simulations and compared the results to these for a similar flexible model. The combination of the chain increment and configurational-bias methods has been applied to calculate the chain chemical potentials. It is found that, at the same density, semiflexible chains have more intermolecular contacts than the fully flexible chains, consistent with previous work.[7] They also exhibit higher volatility and higher chain chemical potentials. As a result, phase envelopes of the semiflexible chains fall below and within the fully flexible counterparts. The critical point temperatures of longer semiflexible chains shift down slightly more than chains of shorter lengths.

Acknowledgment. At Cornell University, research on which this paper is based was supported by a grant from the Department of Energy (Office of Basic Energy Sciences). A.Z.P. is a Camille and Henry Dreyfus Teacher-Scholar. We thank the Cornell Theory Center for SP2 time allocation. At Penn State University this research was funded by the National Science Foundation under Grant No. CTS-9311915.

References and Notes

(1) Mooij, G. C. A. M.; Frenkel, D.; Smit, B. *J. Phys.: Condens. Matter* **1992**, *4*, L255.
(2) Sheng, Y.-J.; Panagiotopoulos, A. Z.; Kumar, S. K.; Szleifer, I. *Macromolecules* **1994**, *27*, 400.
(3) Milchev, A.; Paul, W.; Binder, K. *J. Chem. Phys.* **1993**, *99*, 4786.
(4) Wichert, J. M.; Hall, C. K. *Macromolecules* **1994**, *27*, 2744.
(5) Li, X.-J.; Chiew, Y. C. *Chem. Eng. Sci.* **1994**, *49*, 2805.
(6) Baumgärtner, A. *J. Chem. Phys.*, **1980**, *72*, 871.
(7) Honnell, K. G.; Curro, J. G.; Schweizer, K. S. *Macromolecules* **1990**, *23*, 3496.
(8) Gao, J.; Weiner, J. H., *J. Chem. Phys.* **1989**, *91*, 3168.
(9) Kremer, K.; Grest, G. S. *J. Chem. Phys.* **1990**, *92*, 5057.
(10) Gerroff, I.; Milchev, A.; Binder, K.; Paul. W. *J. Chem. Phys.* **1993**, *98*, 6526.
(11) Curro, J. G.; Schweizer, K. S. *Macromolecules* **1990**, *23*, 1402.
(12) Yethiraj, A.; Kumar, S. K.; Hariharan, A.; Schweizer, K. S. *J. Chem. Phys.* **1994**, *100*, 4691.
(13) Bates, F. S.; Schulz, M. F.; Rosedale, J. H.; Almdal, K. *Macromolecules*, **1992**, *25*, 5547.
(14) Liu, A. J.; Fredrickson, G. H. *Macromolecules* **1992**, *25*, 5551.
(15) Siepmann, J. I.; Karaborni, S.; Smit, B. *Nature* **1993,** *365*, 330.
(16) Kumar, S. K.; Szleifer, I.; Panagiotopoulos, A. Z. *Phys. Rev. Lett.* **1991**, *66*, 2935.
(17) Frenkel, D.; Mooij, G. C. A. M.; Smit, B. *J. Phys.: Condens. Matter* **1992**, *3*, 3053.
(18) Frenkel, D.; Smit, B. *Mol. Phys.* **1991**, *75*, 983.
(19) Rigby, D.; Roe, R. J. In Chapter 6 *Computer Simulation of Polymers*; Roe, R. J., Ed.; Prentice-Hall International Editions; Prentice-Hall: Englewood Cliffs, NJ, 1991.
(20) de Pablo, J. J.; Laso, M.; Suter, U. W. *J. Chem. Phys.* **1992**, *96*, 6157.
(21) Hansen, J-P.; Verlet, L. *Phys. Rev.* **1969**, *184*, 151.
(22) Weinhold, J. Material Science, Penn State University, private communication, 1995.

MA951343Y